REPORT DOCUMENTATION PAGE

Form Approved
OMB No. 0704-0188

1. REPORT DATE *(DD-MM-YYYY)*	2. REPORT TYPE	3. DATES COVERED *(From - To)*
21-07-2008	Journal Article	

4. TITLE AND SUBTITLE

Measurement of Transient Heat Flux and Surface Temperature Using Embedded Temperature Sensors (Postprint)

5a. CONTRACT NUMBER

5b. GRANT NUMBER

5c. PROGRAM ELEMENT NUMBER

6. AUTHOR(S)
Edward Coy (AFRL/RZSA)

5d. PROJECT NUMBER

5e. TASK NUMBER
50260548

5f. WORK UNIT NUMBER

7. PERFORMING ORGANIZATION NAME(S) AND ADDRESS(ES)

Air Force Research Laboratory (AFMC)
AFRL/RZSA
10 E. Saturn Blvd.
Edwards AFB CA 93524-7680

8. PERFORMING ORGANIZATION REPORT NUMBER

AFRL-RZ-ED-JA-2008-308

9. SPONSORING / MONITORING AGENCY NAME(S) AND ADDRESS(ES)

Air Force Research Laboratory (AFMC)
AFRL/RZS
5 Pollux Drive
Edwards AFB CA 93524-7048

10. SPONSOR/MONITOR'S ACRONYM(S)

11. SPONSOR/MONITOR'S NUMBER(S)
AFRL-RZ-ED-JA-2008-308

12. DISTRIBUTION / AVAILABILITY STATEMENT

Approved for public release; distribution unlimited (PA #08295A).

13. SUPPLEMENTARY NOTES

Published in the AIAA Journal of Thermophysics and Heat Transfer, Vol. 24, No. 1, January-March 2010.

14. ABSTRACT

A method for resolving inverse heat conduction problems using approximating polynomials is described. The coefficients are obtained by constraining the even-numbered spatial derivatives of the polynomial at two points within the domain using the heat equation. The result is a linear time-invariant system that can be implemented as a digital filter and is suitable for application in a real-time sensor. The method places no restrictions on boundary or initial conditions, and temperature dependence of transport properties is accounted for in an approximate way. The performance of the model has been validated using analytical and numerical solutions, and results are presented in the frequency and time domains for several orders of polynomials. A propagation of error analysis is presented and is used to establish the optimum location of the sensors.

15. SUBJECT TERMS

16. SECURITY CLASSIFICATION OF:			17. LIMITATION OF ABSTRACT	18. NUMBER OF PAGES	19a. NAME OF RESPONSIBLE PERSON
					Dr. Edward Coy
a. REPORT	b. ABSTRACT	c. THIS PAGE			19b. TELEPHONE NUMBER *(include area code)*
Unclassified	**Unclassified**	**Unclassified**	SAR	9	N/A

JOURNAL OF THERMOPHYSICS AND HEAT TRANSFER
Vol. 24, No. 1, January–March 2010

Measurement of Transient Heat Flux and Surface Temperature Using Embedded Temperature Sensors

Edward B. Coy*
U.S. Air Force Research Laboratory, Edwards Air Force Base, California 93524

DOI: 10.2514/1.45075

A method for resolving inverse heat conduction problems using approximating polynomials is described. The coefficients are obtained by constraining the even-numbered spatial derivatives of the polynomial at two points within the domain using the heat equation. The result is a linear time-invariant system that can be implemented as a digital filter and is suitable for application in a real-time sensor. The method places no restrictions on boundary or initial conditions, and temperature dependence of transport properties is accounted for in an approximate way. The performance of the model has been validated using analytical and numerical solutions, and results are presented in the frequency and time domains for several orders of polynomials. A propagation of error analysis is presented and is used to establish the optimum location of the sensors.

Nomenclature

a_{ij}	=	matrix of location-dependent coefficients, a_{13}, a_{14}:m^2; a_{21}, a_{22}:m^{-1}; a_{23}, a_{24}:m; a_{43}, a_{44}:m^{-1}
$b_j(t)$	=	vector of temperature measurements, b_1, b_2:K; b_3, b_4:K/m^2
$c_i(t)$	=	vector of temperature profile polynomial coefficients, c_1:K; c_2: K/m; c_3:K/m^2; c_4:K/m^3
c_p	=	heat capacity, $J/kg \cdot K$
Im	=	imaginary part
i	=	imaginary number, $\sqrt{-1}$
k	=	thermal conductivity, $W/m \cdot K$
P_n	=	temperature profile polynomial of degree n, K
q	=	heat flux, W/m^2
Re	=	real part
T	=	temperature, K
$\dot{T}$	=	rate of change of temperature, K/s
t	=	time, s
x	=	distance from the surface, m
α	=	thermal diffusivity, m^2/s
β_j	=	low-pass filter coefficient for time derivative, s^{-1}
Γ	=	gain, nondimensional
γ_j	=	low-pass filter coefficient for time average
Δt	=	time step, s
δ	=	uncertainty
ρ	=	density, kg/m^3
σ	=	length scale parameter, m^{-1}
ϕ	=	phase angle, rad
ω	=	angular frequency, rad/s
$\|\ \|$	=	amplitude

Subscripts

i, j	=	polynomial and matrix indices
m	=	low-pass filter index
n	=	order of polynomial approximation for temperature
1	=	position nearest to the measurement surface
2	=	position farthest from the measurement surface
%	=	nondimensional number

Superscripts

~	=	frequency domain quantity
-	=	low-pass filtered quantity
*	=	complex conjugate

I. Introduction

THE measurement of the transient heat flux and the surface temperature in heat-sink combustion chambers continues to present technical challenges to the instrumentation engineer. Sensor failure rates are high, and measurement accuracies and uncertainties are not well characterized. These shortcomings have had a significant impact on some recent programs that have used heat-sink test articles to acquire data for the validation of heat transfer predictions at liquid rocket engine operating conditions [1,2].

There are numerous types of heat flux sensors, but a relatively small subset is capable of operating in rocket chamber conditions in which the heat flux levels can exceed 10^8 W/m^2, and the surface temperatures of 1000 K are typical. Diller [3] reviewed the devices that have been used and organized them into methods that relied on temperature differences over a spatial distance with known thermal resistance and temperature differences over time having known thermal capacitance. The most commonly used method has been the coaxial thermocouple, which is an example of the second type. A thermocouple junction is formed on the surface of the chamber between a wire of one type of thermocouple material and a surrounding sheath of another type. The heat flux is determined from the measured temperature boundary condition using a one-dimensional transient solution to the heat equation. The junction is typically a few micrometers in thickness and is often formed by lightly scratching the surface to drag filaments of one type of material across the electrically insulating layer to the other type. In some applications, when erosion of the surface occurs, the junction is continuously reformed, and this has led to the description of coaxial thermocouples as eroding thermocouples. However, in heat-sink chambers, it is quite common to find that the junction disappears at some point during a test, and the sensor fails.

Other methods have been developed that do not rely on surface temperature measurements but embed the sensors within the wall where they are protected from erosion. In the null-point calorimeter, a hole is drilled from the backside of the chamber wall and a thermocouple is inserted. The bead is brazed or resistance welded to the bottom of the hole. Null point refers to a distance from the bottom of the hole to the inner wall, where the disturbance to the flow of heat caused by the hole results in the junction reading nearly equal to the

Presented as Paper 3952 at the AIAA 26th Ground Test and Aerodynamics Measurements, Seattle, WA, received 21 April 2009; accepted for publication 12 September 2009.

*Propulsion Research Engineer, Aerophysics Branch, Space and Missiles Propulsion Division, Propulsion Directorate, 10 East Saturn Boulevard. Member AIAA.

inner wall temperature. The construction of null-point calorimeters is challenging. The junction cannot be visually inspected, and large measurement errors can result from manufacturing flaws [4].

Another method using embedded temperature sensors is the plug-type heat flux gauge of Liebert [5]. An annular groove is machined into the chamber wall to form a post, and thermocouples are attached at several axial points along the outside of the post. A polynomial curve is used to extrapolate the temperatures to the wall position, and an integral method is used to calculate the total heat load to the plug from transient temperature measurements. Two-dimensional effects can be significant in this type of device. The dimensions of the groove are critical, and significant errors can result from the disturbance to the flow of heat [6].

Recently, Conley et al. used embedded temperature sensors to measure transient heat flux in a subscale combustion chamber [7]. Transient temperature data were reduced to heat flux using an equation developed from an energy balance on a control volume between the sensors. The equation includes terms for Fourier's law of heat conduction and heat storage. Nominal constant values were used for the properties.

The data reduction methods developed by Leibert [5] and Conley et al. [7] are particular examples of a more general class of inverse solution procedures. Inverse heat transfer problems are challenging because surface conditions must be obtained from temperature sensors embedded within objects that experience attenuated and time-lagged responses to changes in the boundary conditions. Solution methods must be stable and accurate in the presence of noisy signals. Most inverse methods are based on minimizing the sum of square residuals (SSR) of the difference between measurements and a solution of the heat equation. An initial estimate is made for the boundary condition, and the response at the sensor location is calculated. Then the estimate is improved using a gradient method until a convergence criterion for SSR is satisfied. The method used to calculate the response is specific to the problem and can be any of the analytical and numerical methods that exist for solving the heat equation. However, there is a fundamental physical limit on the size of the time step because there must be sufficient time for the change in the boundary to propagate to the sensor location. A primary focus of research in this area is the development of methods that can achieve the smallest possible time step without incurring instability. A widely used procedure is the function specification method [8]. A functional form for the time dependence of the boundary condition is assumed. and the parameters of the function are then determined by minimizing SSR. The function may span the entire time domain or it may be parsed into subintervals. Another widely used class of technique is based on regularization [8]. These techniques add additional factors to the least squares function to enhance stability and convergence.

If the method used to solve the heat equation is a numerical technique, the number of processor operations will likely require that the inverse calculations be performed as a postprocessing operation. However, if the method is based on an analytical solution, it may be possible to perform the calculation in real time. Inverse methods based on analytical solutions are generally limited to situations for which thermal properties are effectively constant and specific boundary conditions are satisfied. An important subset of these methods has been developed for the case in which the transient surface temperature is measured and the test duration is short, such that the body can be treated as an infinitely thick slab. The method of Cook and Felderman assumes that heat flux is constant within a sampled time interval and the analytical relation between heat flux and surface temperature is used to obtain the surface flux from the measured temperatures as a summation of contributions from each time interval [9]. Cook also suggested a modification to the method to account for temperature-dependent properties [10].

There have been a number of publications describing the application of digital signal processing techniques to the measurement of heat transfer. Beck et al. discusses the use of an efficient digital filter algorithm for linear problems and its application to online or real-time data processing [8]. In the method by Beck et al., the filter coefficients can be derived for the particular problem from any of the numerical or analytical approaches. Once obtained, the filter coefficients do not change, and the heat flux calculation is reduced to the product of two arrays, although a specific origin of time is required. Marineau and Hornung described an efficient method for calculating heat flux from surface temperature measurements based on digital signal processing techniques [11]. The relationship between heat flux and surface temperature is based on the Green's function for the impulse problem, and the heat flux is deconvolved from the Green's function and the surface temperature in the frequency domain. Oldfield developed an efficient method for processing signals from thin film heat flux gauges based on the linear time-invariant (LTI) system theory [12]. The analytical solution for the impulse response of the sensor is convolved with the measured temperature distribution to obtain the surface heat flux.

Frankel et al. have suggested other approaches that could be used for real-time processing [13]. For a one-dimensional problem, a Taylor series can be used to extrapolate from the measurement point to the surface condition, with the spatial derivatives in the series obtained from rate sensors for temperature and heat flux (which is nonintrusive to the flow of heat) and the heat equation. Frankel also suggested a two-sensor arrangement , wherein a Taylor series for the first sensor is expanded about location x, and a series for the second sensor is expanded about $2x$. Adding the two expansions eliminates terms and results in an order of accuracy equal to the one sensor expansion, with derivatives in time one order lower.

In this paper, we extend these ideas and report a number of new results for the class of methods based on the extrapolation of a function for the two-sensor arrangement. We have found that this method leads to very satisfactory solutions to the major technical challenges of accuracy, time response, stability in the presence of noise, uncertainty, computational efficiency, failure rate, and producibility in the heat-sink chambers used for rocket heat transfer experiments.

II. Derivation of Model

The domain of interest is a continuous one-dimensional body with smoothly varying or constant thermal properties (Fig. 1). The initial temperature distribution is assumed to be continuous and smoothly varying. The boundary conditions at the surfaces are arbitrary and may be discontinuous in time. The principle goal of the analysis is to determine the transient temperature and heat flux at $x = 0$ from temperature data at x_1 and x_2.

We begin by assuming a one-dimensional flow of heat in the x direction and approximate the temperature profile in the body with a polynomial in x with time-dependent coefficients:

$$P_n(x,\ t) = \sum_{i=1}^{n+1} c_i(t) x^{i-1} \tag{1}$$

In addition to matching temperatures at the two points, the polynomial is also required to satisfy the one-dimensional heat equation. Specifically, it is required to match the second derivative of temperature with respect to position:

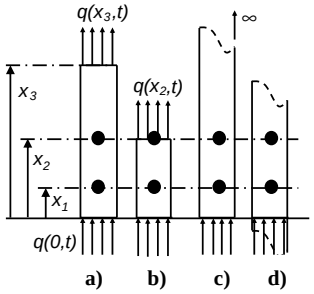

Fig. 1 Domains addressed by current theory: a) finite slab, b) finite slab with sensor on second surface, c) semi-infinite slab, and d) internal points.

$$\frac{\partial^2 T}{\partial x^2} = \frac{1}{\alpha}\frac{\partial T}{\partial t} \tag{2}$$

As shown by Burggraf [15], the heat equation can be extended to any even-numbered derivative of x:

$$\frac{\partial^{2m} T}{\partial x^{2m}} = \frac{1}{\alpha^m}\frac{\partial^m T}{\partial t^m}, \qquad m = 1,\ 2,\ \ldots \tag{3}$$

Expressions for the $c_i(t)$ in Eq. (1) are obtained by equating $P_n(x,\ t)$ and its even-numbered spatial derivatives with measured values. For the case of $P_3(x,\ t)$, the set of equations can be expressed in matrix form as follows:

$$\begin{bmatrix} T(x_1,\ t) \\ T(x_2,\ t) \\ \frac{\partial^2 T(x_1,\ t)}{\partial x^2} \\ \frac{\partial^2 T(x_2,\ t)}{\partial x^2} \end{bmatrix} = \begin{bmatrix} 1 & x_1 & x_1^2 & x_1^3 \\ 1 & x_2 & x_2^2 & x_2^3 \\ 0 & 0 & 2 & 6x_1 \\ 0 & 0 & 2 & 6x_2 \end{bmatrix} \begin{bmatrix} c_1(t) \\ c_2(t) \\ c_3(t) \\ c_4(t) \end{bmatrix} \tag{4}$$

The inverse is the following:

$$\begin{bmatrix} c_1(t) \\ c_2(t) \\ c_3(t) \\ c_4(t) \end{bmatrix} = \begin{bmatrix} \frac{x_2}{x_2-x_1} & \frac{-x_1}{x_2-x_1} & \frac{x_1x_2(2x_2-x_1)}{6(x_2-x_1)} & \frac{x_1x_2(x_2-2x_1)}{6(x_2-x_1)} \\ \frac{-1}{x_2-x_1} & \frac{1}{x_2-x_1} & \frac{x_1^2-2x_1x_2-2x_2^2}{6(x_2-x_1)} & \frac{2x_1^2+2x_1x_2-x_2^2}{6(x_2-x_1)} \\ 0 & 0 & \frac{x_2}{2(x_2-x_1)} & \frac{-x_1}{2(x_2-x_1)} \\ 0 & 0 & \frac{-1}{6(x_2-x_1)} & \frac{1}{6(x_2-x_1)} \end{bmatrix} \begin{bmatrix} T(x_1,t) \\ T(x_2,t) \\ \frac{\partial^2 T(x_1,t)}{\partial x^2} \\ \frac{\partial^2 T(x_2,t)}{\partial x^2} \end{bmatrix} \tag{5}$$

$$c_i(t) = a_{ij} b_j(t) \tag{6}$$

All terms in a_{ij} depend only on the sensor locations and need to be calculated once. The vector $b_j(t)$ contains the experimental measurements. The second derivative terms in $b_j(t)$ are obtained from Eq. (2). The method used to calculate the time derivative in Eq. (2) is critical to the success of the technique because differentiation of experimental data can be a highly unstable process [13,14,16,17] and low-pass filtering is usually required. The vector $c_i(t)$ can be used to reconstruct an approximation for the temperature profile in the sensor, but the most important application is in the estimate of the boundary conditions:

$$T(0,t) \approx P_3(0,t) = c_1(t) \tag{7}$$

$$q(0,\ t) \approx -k\frac{\partial P_3(0,\ t)}{\partial x} = -kc_2(t) \tag{8}$$

Note that there are no specific limitations that have been placed on the boundary conditions. The model can be applied to semi-infinite or finite thickness slabs. The sensor at x_2 can be embedded in the body or it can be placed on the surface. The surface can be adiabatic or actively cooled at a known or unknown rate. The technique can be used to estimate temperature and heat flux profiles within a body. The extension of this approach to higher-order polynomials, using Eq. (3), and radial geometry is straightforward.

As an initial illustration of the ability of the polynomial approximations to reproduce temperature profiles and boundary conditions, we take as an example a uniform slab of copper exposed to a steady-periodic heat flux boundary condition. The heat flux is oscillating sinusoidally at 10 Hz, and temperature sensors are located at depths of 2 and 5 mm from the heated surface. For the purpose of this illustration, the sensors are free of noise. In Fig. 2, the analytical solution is compared with polynomial approximations of orders 1, 3 and 5. The order 1 approximation is a simple linear extrapolation of temperature to the surface. It is, in effect, a steady approximation and exhibits a large error and time delay. The maximum fractional error at the surface, based on the amplitude of the input wave, is 0.81. The order 3 approximation includes the second derivative terms, and the results are much improved. The maximum fractional error at the surface is reduced to 0.11. The order 5 approximation includes second and fourth derivatives and is indistinguishable from the exact solution. The maximum fractional error at the surface is 0.03.

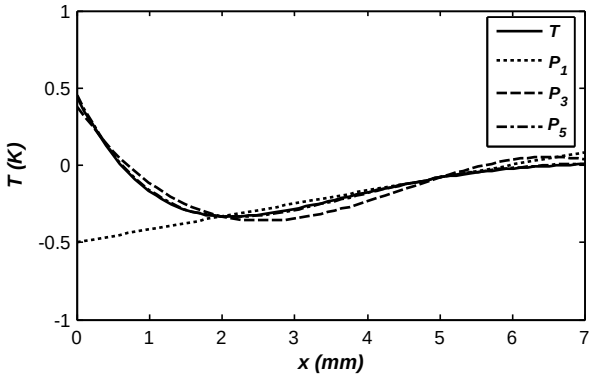

Fig. 2 Polynomial approximations to temperature profile in a copper slab exposed to steady-periodic heat flux at left boundary. Sensors are located at 2 and 5 mm.

A. Frequency Domain Analysis

The equations in (5) constitute an LTI system. The polynomial approximation is obtained from linear combinations of the measurements contained in the $b_j(t)$ vector with the constant coefficients of the a_{ij} matrix. The system is time invariant because the output is based on current values of the measurements only. Therefore, a time shift in the input produces an equal time shift in the output. LTI systems can be completely represented by an impulse response or equivalently, in the frequency domain, by the gain and phase response. In this section, we present the frequency domain behavior for approximating polynomials of orders 1, 3, and 5. To avoid lengthy expressions, we illustrate the transformation using just the P_3 approximation. We begin with the following expression for the time-domain surface temperature, which has been obtained by replacing the second derivatives with respect to x in the $b_j(t)$ vector with the right-hand side of Eq. (2):

$$P_3(0,t) = a_{11}T(x_1,t) + a_{12}T(x_2,t) + a_{13}\frac{\dot{T}(x_1,t)}{\alpha} + a_{14}\frac{\dot{T}(x_2,t)}{\alpha} \tag{9}$$

Following Cole, we transform to the frequency domain using the complex-valued $\tilde{T}(x,\omega)$ [18]:

$$T(x,\ t) = Re[\tilde{T}(x,\ \omega)e^{i\omega t}] \tag{10}$$

Substituting Eq. (10) into Eq. (9),

$$\tilde{P}_3(0,\ \omega) = \left(a_{11} + i\frac{\omega}{\alpha}a_{13}\right)\tilde{T}(x_1,\ \omega) + \left(a_{12} + i\frac{\omega}{\alpha}a_{14}\right)\tilde{T}(x_2,\ \omega) \tag{11}$$

The corresponding expression for surface heat flux is

$$-k\frac{\partial \tilde{P}_3(0,\ \omega)}{\partial x} = -k\left[\left(a_{21} + i\frac{\omega}{\alpha}a_{23}\right)\tilde{T}(x_1,\ \omega) + \left(a_{22} + i\frac{\omega}{\alpha}a_{24}\right)\tilde{T}(x_2,\ \omega)\right] \tag{12}$$

To illustrate the behavior of the model, we obtain inputs from an exact analytical solution. We consider the case of a uniform semi-infinite slab with a steady-periodic heat flux boundary condition. The solution to this problem is [19]:

$$\tilde{T}(x,\ \omega) = \frac{|q|}{k}\frac{e^{-\sigma x}}{\sigma}, \qquad (0 \le x < \infty,\ \omega \ge 0) \tag{13}$$

$$\tilde{q}(x,\ \omega) = |q|e^{-\sigma x}, \qquad (0 \le x < \infty,\ \omega \ge 0) \tag{14}$$

$$\sigma = (1 + i)\sqrt{\frac{\omega}{2\alpha}} \tag{15}$$

Gain is defined as the ratio of the amplitude of the model to the actual value:

$$\Gamma(P_n) = |\tilde{P}_n(0, \omega)|/|\tilde{T}(0, \omega)| \tag{16}$$

Phase is defined as the difference between the phase of the model and the actual value:

$$\phi(P_n) = \tan^{-1}\left(\frac{\mathrm{Im}[\tilde{P}_n(0, \omega)]}{Re[\tilde{P}_n(0, \omega)]}\right) - \tan^{-1}\left(\frac{\mathrm{Im}[\tilde{T}(0, \omega)]}{Re[\tilde{T}(0, \omega)]}\right) \tag{17}$$

The gain and phase expressions for surface heat flux are identical to those for surface temperature.

Gain and phase plots are shown in Figs. 3–6 for polynomials of orders 1, 3, and 5. Frequency has been nondimensionalized using a time scale based on the thermal diffusivity and the depth of the near-surface sensor:

$$\omega_{\%} = \frac{x_1^2 \omega}{\alpha} \tag{18}$$

The value of x_2/x_1 in each case is 2.3. This value was determined to be near optimal and is discussed further, next, in the context of the noise sensitivity. The gain behavior for surface temperature is shown in Fig. 3. All orders of approximation converge to a gain of one at low frequency but deviate as frequency is increased. The P_1 approximation rolls off slowly to zero and has a -3 db frequency of 2. The P_3 approximation exhibits a region of gain greater than 1 and then rolls off at a frequency of 20. The P_5 approximation has a larger gain region and a -3 dB frequency of 100. The region of gain greater than one can be eliminated by low-pass filtering, as will be shown later. The gain at high frequency would manifest itself in the time domain as an overshoot in the response when subjected to rapid changes in the inputs. The phase behaviors show similar points of departure, but all approximations exhibit monotonically increasing phase lag (Fig. 4). From these plots, we can state that the P_3 approximation has a frequency response approximately one order of magnitude higher than the P_1 approximation, and the P_5 approximation is approximately two orders higher.

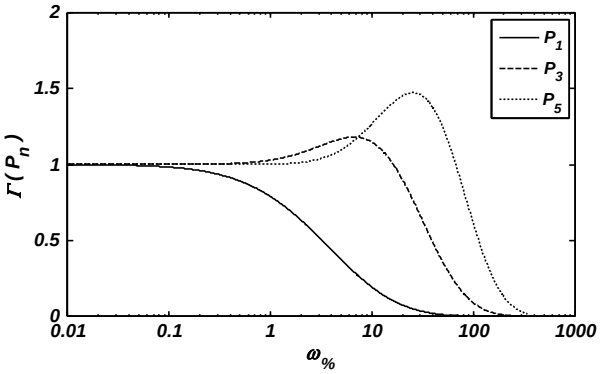

Fig. 3 Surface temperature gain for three orders of polynomial models.

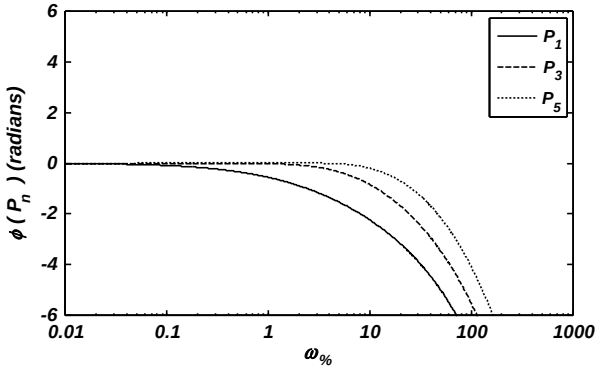

Fig. 4 Surface temperature phase for three orders of polynomial models.

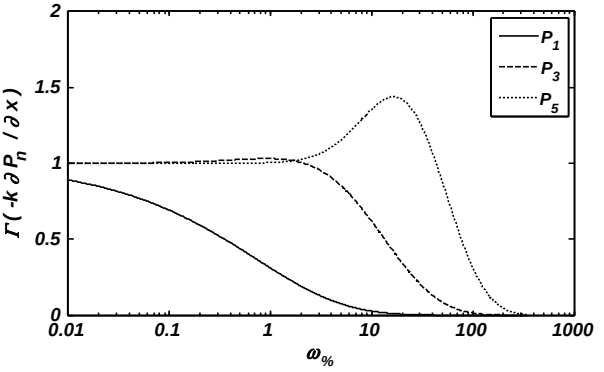

Fig. 5 Surface heat flux gain for three orders of polynomial models.

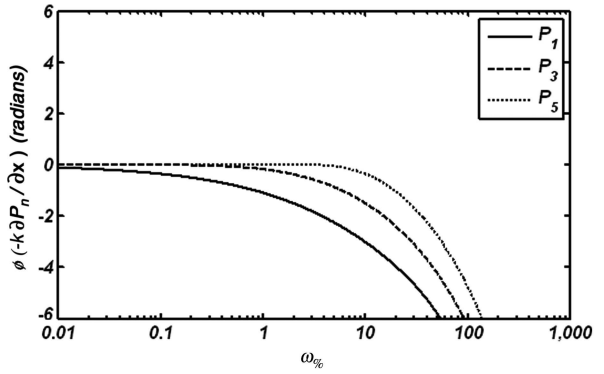

Fig. 6 Surface heat flux phase for three orders of polynomial models.

The behavior of the surface heat flux plot (Fig. 5) is qualitatively similar to surface temperature, but the points of departure and roll off are shifted to lower frequencies. The -3 db point of the P_1 approximation occurs at a frequency of 0.3 because the simple linear extrapolation does a poor job capturing the slope of the temperature profile at the surface. The P_3 approximation shows smaller amplitude in the gain region than the surface temperature plot, but the P_5 approximation continues to have a region of large gain. The phase characteristics of heat flux are also monotonically decreasing (Fig. 6). The point of departure for P_1 is shifted to a frequency of less than 0.01. The P_3 approximation begins to exhibit a phase lag at a frequency of 0.3, but the P_5 does not exhibit a phase lag until 20. From these plots, we can state that the P_3 approximation has a frequency response at least three orders of magnitude higher than the P_1 approximation, and the P_5 approximation is approximately four orders higher. These improvements come about solely as a result of a higher-order polynomial approximation to the temperature profile.

B. Low-Pass Filtering

The formulation as an LTI system facilitates the use of digital signal processing techniques. Low-pass filtering of the input signals can improve the performance of the polynomial models by suppressing the propagation of errors from the input signals and by eliminating the region of gain greater than one. The design of optimum filters is an extensive subject and has been treated by several authors in the context of inverse heat conduction methods. Hensel showed that filtering the input data improves the stability of an inverse calculation, and he recommended the use of a Gaussian filter because it does not distort phase and has an acceptable rate of roll off

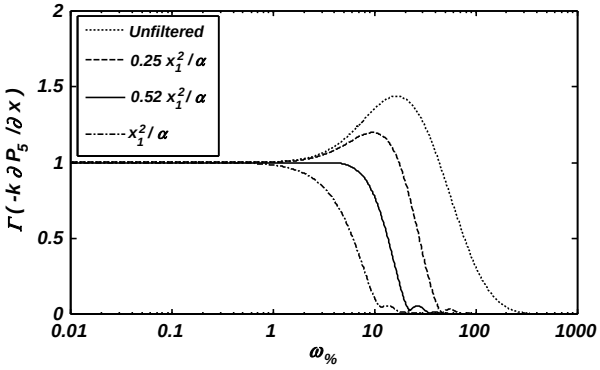

Fig. 7 Heat flux gain for P_5 model with low-pass filter for four values of filter window width.

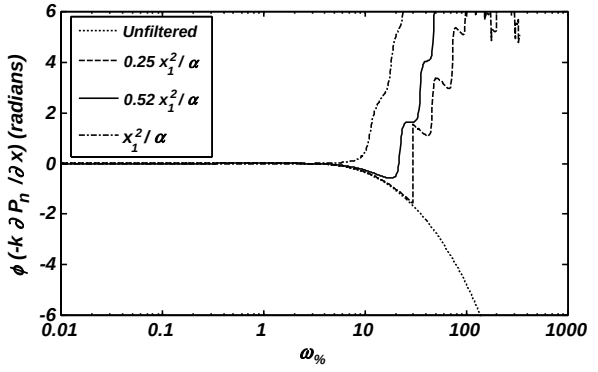

Fig. 8 Heat flux phase for P_5 model with low-pass filter for four values of filter window width.

at high frequency [20]. Frankel used a Gaussian filter to suppress noise in the input signals before using a finite difference calculation to obtain a time derivative [14]. Frankel suggested a method for interrogating the power spectrum to locate an optimum cutoff frequency for the input filter. However, there remained a significant propagation of error to the derivative, which he attributed to the ill-posed nature of numerically differentiating noisy data [14].

An important factor in choosing a low-pass filter, in addition to the phase and roll-off characteristics, is the efficiency with which the calculation can be performed. The most efficient methods are implemented as convolutions in the time domain:

$$\bar{T}(x_i,\, t_n) = \sum_{j=-m}^{m} \gamma_j T(x_i,\, t_{n+j}) \tag{19}$$

$$\bar{\dot{T}}(x_i,\, t_n) = \sum_{j=-m}^{m} \beta_j T(x_i,\, t_{n+j}) \tag{20}$$

A filter that is well suited for this type of processing is the polynomial smoothing filter, also known as the Savitzky–Golay filter [21,22]. The linear combination of the coefficients γ_j and β_j, with the data $T(x_i,\, t_{n+j})$, results in filtered values that are identical to those obtained from a least squares fit of a polynomial. However, the filter is computationally efficient because it eliminates the need for a matrix inversion.

It is informative to transform the low-pass filter into the frequency domain in order to characterize the effect on the gain and phase behavior of the polynomial model. This is accomplished by applying the discrete Fourier transform to Eqs. (19) and (20) and then using the filtered frequency domain temperatures in Eqs. (11) and (12) [23]. The effect of a quadratic polynomial filter on the heat flux response is shown in Figs. 7 and 8 for the P_5 model. The figures contain curves for four values of the filter window width based on the characteristic time scale for the diffusion of heat x_1^2/α. The window width of $0.25\alpha/x_1^2$ is too narrow to remove the high frequencies in which the gain is greater than one. The window width of $0.52\alpha/x_1^2$ removes the region of gain greater than one and approaches most closely to the ideal gain curve. Further increasing the window width to x_1^2/α reduces the frequency response by approximately a factor of 3. The filter introduces characteristic high frequency modes, and these are sometimes cited as a drawback of the Savitzky–Golay filter. However, for this application, although the modes create large errors in phase above a frequency of 20, the gain is negligible and the results are not significantly affected.

C. Efficiency

The main advantage of the current method over the more general inverse methods is that it can be formulated as a digital filter and calculated in the time domain with relatively few processor operations. To obtain the minimum number of operations, the filter coefficients can be combined with the a_{ij} coefficients. Using the P_3 case as an example, Eqs. (19) and (20) can be substituted into Eq. (5) to obtain the following forms for the surface temperature and heat flux:

$$P_3(0,\, t_n) = \sum_{j=-m}^{m} \left[\left(a_{11}\gamma_j + \frac{a_{13}}{\alpha}\beta_j \right) T(x_1,\, t_{n+j}) + \left(a_{12}\gamma_j + \frac{a_{14}}{\alpha}\beta_j \right) T(x_2,\, t_{n+j}) \right] \tag{21}$$

$$-k\frac{\partial P_3(0,\, t_n)}{\partial x} = -k \sum_{j=-m}^{m} \left[\left(a_{21}\gamma_j + \frac{a_{23}}{\alpha}\beta_j \right) T(x_1,\, t_{n+j}) + \left(a_{22}\gamma_j + \frac{a_{24}}{\alpha}\beta_j \right) T(x_2,\, t_{n+j}) \right] \tag{22}$$

The coefficients multiplying the temperatures can be calculated once, and then only $4m + 2$ multiplications and $2m + 1$ additions are required to evaluate surface temperature and heat flux (or about 100 processor operations for a typical value of $m \approx 10$). As an illustration, Figs. 9–11 contain coefficients for 31 point filters for surface heat flux for polynomials of orders 1, 3 and 5, respectively. Note also that the number of operations is not affected by the order of the approximating polynomial. The order affects only the value of the coefficients.

D. Noise Sensitivity

The propagation of noise from the temperature measurements to the predicted surface temperature and heat flux can be evaluated by treating each temperature measurement as an independent random variable and using the square-root-of-sum-of-squares approach for error propagation [24]. In the following, we assume that the uncertainty in temperature measurement δT is the same at the two measurement locations, and the uncertainties in measurement positions and material properties are negligible. Proceeding from Eqs. (21) and (22) for the P_3 approximation, we have

$$\delta P_3(0,\, t_n) = \left[\sum_{i=-m}^{m} \left(a_{11}\gamma_j + \frac{a_{13}}{\alpha}\beta_j \right)^2 \delta T^2 + \left(a_{12}\gamma_j + \frac{a_{14}}{\alpha}\beta_j \right)^2 \delta T^2 \right]^{1/2} \tag{23}$$

$$\delta\left(k\frac{\partial P_3(0,\, t_n)}{\partial x} \right) = k[P_3(0,\, t_n)] \left[\sum_{i=-m}^{m} \left(a_{21}\gamma_j + \frac{a_{23}}{\alpha}\beta_j \right)^2 \delta T^2 + \left(a_{22}\gamma_j + \frac{a_{24}}{\alpha}\beta_j \right)^2 \delta T^2 \right]^{1/2} \tag{24}$$

Equations (23) and (24), as well as the equivalent equations for the other orders of approximation, can be rewritten in terms of the

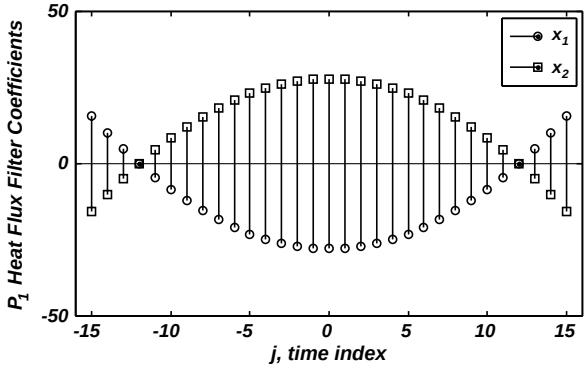

Fig. 9 Coefficients for calculation of surface heat flux based on P_1 approximation.

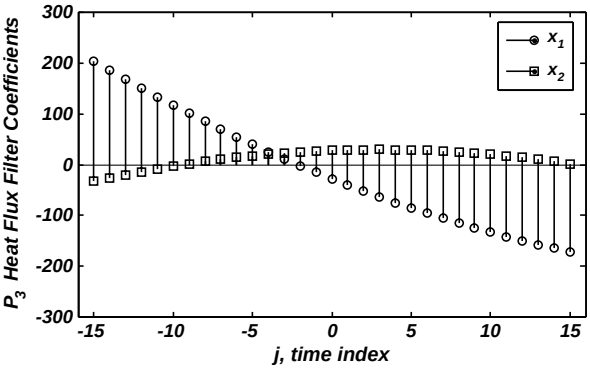

Fig. 10 Coefficients for calculation of surface heat flux based on P_3 approximation.

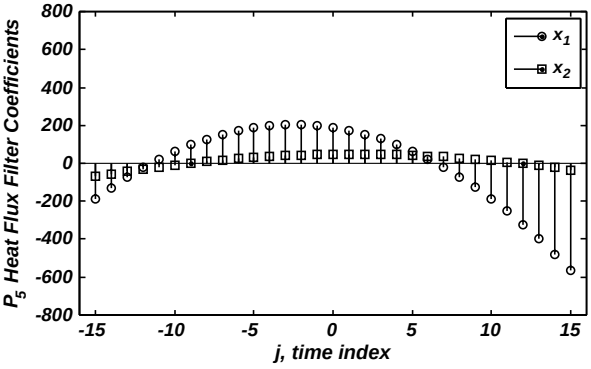

Fig. 11 Coefficients for calculation of surface heat flux based on P_5 approximation.

following signal-to-noise ratios, such that the only independent variables are the depth ratio x_2/x_1 and the filter parameters. The filter parameters used in producing the plots were those for a quadratic smoothing function with a window width of $0.52\alpha/x_1^2$ and $m = 10$. The particular values are not significant because we are primarily interested in the relative levels of noise for the three approximations. Noise levels on the inputs can always be reduced by increasing the sampling rate in order to obtain more points within the specified time window:

$$\delta T_{\%} = \frac{\delta P_n(0,\ t)}{\delta T} \tag{25}$$

$$\delta q_{\%} = \frac{\delta(k\partial P_n/\partial x)}{k\delta T/x_1} \tag{26}$$

Figures 12 and 13 contain the results for the three orders of approximation plotted as functions of the depth ratio of the sensors x_2/x_1. The noise increases with the order of the model because the magnitude of the coefficients increases, as can be seen in Figs. 9–11. The P_1 model has the lowest level of noise and it decreases monotonically with the depth ratio. The P_3 and P_5 approximations both exhibit minima with respect to x_2/x_1 for both surface temperature and heat flux. However, the minima are broad, and values in the range of 2.3–2.8 are effectively equivalent. Noise increases for $x_2/x_1 < 2$, and so this range should be avoided. An important observation is that in all cases the noise is bounded. The method is inherently stable because it has the characteristics of a low-pass filter as discussed previously.

E. Temperature-Dependent Properties

The linear form of the heat equation, given in the preceding section as Eq. (2), is valid when thermal properties are constant. However, in many applications temperature dependence is significant. The most basic example is the case of a sensor that undergoes a large temperature change during the period of measurement. In heat-sink rocket chamber experiments, the wall temperature can change by 800 K or more, resulting in a 30% decrease in the thermal diffusivity. Spatial gradients in thermal properties can also be significant. As a first approximation, when the temperatures at the two measurement locations are significantly different, the local temperatures can be used to evaluate the thermal diffusivity and the second derivative term in Eq. (2). An improved approximation including spatial gradients in properties can be obtained through the nonlinear form of the one-dimensional heat equation:

$$\frac{\partial}{\partial x}\left(k\frac{\partial T}{\partial x}\right) = \rho c_p \frac{\partial T}{\partial t} \tag{27}$$

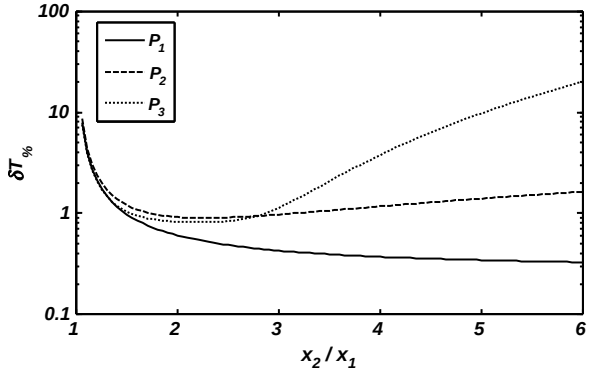

Fig. 12 Noise in surface temperature prediction.

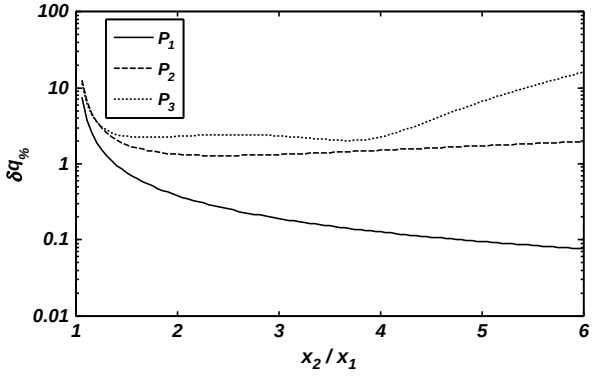

Fig. 13 Noise in heat flux prediction.

In this case, the second derivative becomes

$$\frac{\partial^2 T}{\partial x^2} = \frac{1}{\alpha}\frac{\partial T}{\partial t} - \frac{1}{k}\frac{\mathrm{d}k}{\mathrm{d}T}\left(\frac{\partial T}{\partial x}\right)^2 \tag{28}$$

To a first approximation, the first term on the right-hand side increases proportionally with the heat flux, whereas the second term increases with the heat flux squared. For pure copper, the second term becomes significant when heat flux is on the order of 5×10^7 W/m^2. The temperature gradient in the second term cannot be measured directly but can be estimated from the linear form of the heat equation, and this can be used in Eq. (28) to obtain an improved estimate for the second derivative. The process can be repeated until a convergence criterion is satisfied. Related expressions can be obtained for the higher-order derivatives of Eq. (3); however, the expressions are quite lengthy.

The computational cost of evaluating thermal properties at local conditions is negligible, requiring two calls to a variable properties function per time step. The cost of including temperature gradients is larger. The calculation of the spatial derivatives of temperature points requires the evaluation of all of the $c_i(t)$ coefficients, then new coefficients for the digital filter must be calculated and, finally, the filter calculation must be repeated. The additional steps increase the processing time by approximately a factor of 4. In most cases, the computational time will still be negligible. However, it is possible to include a flag to turn on the gradient calculations only when heat flux exceeds the critical value.

Example calculations were performed to assess the effectiveness of the variable properties approximations. The reference case was a square-wave pulse of heat of duration $4x_1^2/\alpha$. This case is useful for conveying the time response and the accuracy of the methods, and it is an idealized version of the heat flux pattern encountered in tests of heat-sink rocket chambers. Test case data consisting of temperatures at the measurement locations were generated using a numerical solution of the nonlinear heat equation with functions for the temperature-dependent properties of copper. Figure 14 includes results for the P_5 model for three methods of handling thermal properties for a heat flux of 10^7 W/m^2, and Fig. 15 has the same information for 10^8 W/m^2. At 10^7 W/m^2, the effect of property variations for the short duration pulse is negligible, and all approximations give the same result. The rise time is approximately 0.03 s, and the heat flux is reproduced accurately. For this case, the temperature rise at the surface was 113 K in 0.13 s. At 10^8 W/m^2, the effect of variable properties is observable. The constant properties approximation does not converge to the correct value but rises steadily over the duration of the pulse, and the fall time is significantly increased. The local properties approximation more accurately captures the steady plateau, and the fall rate is improved. However, the heat flux is underpredicted by 2–5%. The gradient approximation exhibits the same rise and fall rates as the local properties approximation, and the accuracy is somewhat improved. However, the square profile is not as well defined as it was for a heat flux of 10^7 W/m^2. For this case, the surface temperature increases by approximately 1200 K over 0.13 s.

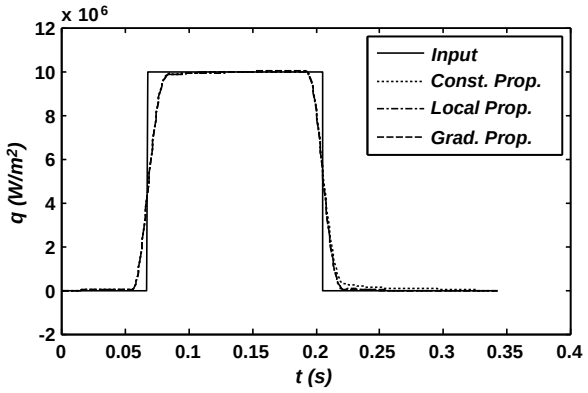

Fig. 14 Effect of temperature-dependent properties on heat flux calculation at 10^7 W/m^2.

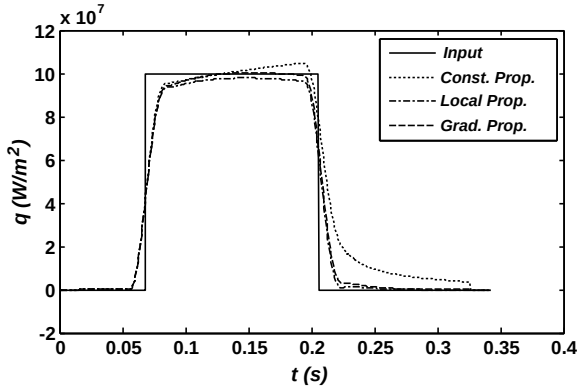

Fig. 15 Effect of temperature-dependent properties on heat flux calculation at 10^8 W/m^2.

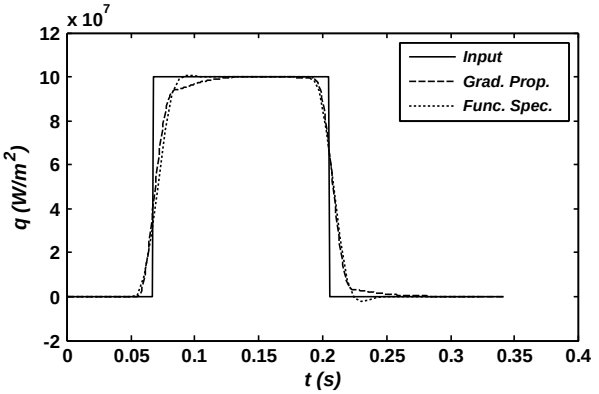

Fig. 16 Comparison with function specification with three future time steps for heat flux of 10^8 W/m^2.

F. Comparison with Beck's Function Specification Method

In this section, we compare the polynomial model with a widely used inverse heat transfer method, the function specification with future time steps method, for a case in which temperature-dependent properties are significant. The method is described fully in [8]. The method was implemented using The MathWorks MATLAB® version 2008 library functions. The pdepe nonlinear equation solver was used to model the heat equation. The pdepe function solves initial-boundary value problems for systems of parabolic and elliptic partial differential equations in one space variable [25]. The spatial domain was divided into forward and inverse regions, and the inverse region between the sensor and the surface consisted of five finite volumes. The fzero function was used to find the minimum of the convergence criteria. The fzero function uses a combination of bisection, secant, and inverse quadratic interpolation methods [26]. The size and number of future time steps were based on optimal values contained in Sec. 5.6.1 of [8]. For the cases described next, the number of time steps was four, and the length of the time step was $0.15x_1^2/\alpha$. Figure 16 contains the results of an example calculation for a heat flux of 10^8 W/m^2. The function specification method accurately reproduces the steady portion of the heat flux and has similar rise and fall times as the P_5 model. The function specification method achieves greater accuracy by modeling the full domain. The computational cost of the higher accuracy in terms of run time was approximately a factor of 10^5 on this example problem.

III. Conclusions

A method has been described for using approximating polynomials to solve the inverse heat transfer problem for the case

of two temperature sensors embedded in the wall of a chamber. The method does not require surface junction thermocouples, which are prone to failure and produce noisy signals in rocket engine flows, and is well suited for studies of the effects of surface features on heat transfer enhancement. An approximating polynomial is constrained to match the temperatures and the even-numbered spatial derivatives at the measurement points. The method requires only current values of temperature and its rate of change, and the boundary and initial conditions are arbitrary. The algorithm can be represented as a low-pass filter, and the gain and phase behavior have been characterized. The placement of the sensors affects the frequency cutoff and the noise response, and optimum values for the relative positions of the sensors have been obtained. The method is computationally efficient, requiring approximately 100 multiply and add operations per measurement, enabling real-time processing in high-channel-count systems.

References

[1] Droppers, L. J., Schuff, R., and Anderson, W., "Study of Heat Transfer in a Gaseous Hydrogen Liquid Oxygen Multi-Element Combustor," AIAA Paper 2007-5550, 2007.

[2] Jones, G., Protz, C., Bullard, B., and Hulka, J., "Local Heat Flux Measurements with Single Element Coaxial Injectors," AIAA Paper 2006-5194, 2006.

[3] Diller, T. E., "Advances in Heat Flux Measurement," *Advances in Heat Transfer*, Vol. 23, Academic Press, New York, 1993, pp. 279–368.

[4] Kidd, C. T., "Recent Developments in High Heat-Flux Measurement Techniques at the AEDC," *Proceedings of 36th International Instrumentation Symposium*, Instrument Society of America, Research Triangle Park, NC, 1992, pp. 35–44.

[5] Liebert, C. H., "Measurement of Local High-Level, Transient Surface Heat Flux," NASA TP-2840, 1988.

[6] Rooke, S., Fralick, G., and Liebert, C., "Heat Transfer Analysis of a Plug-Type Heat Flux Gauge," *Journal of Thermophysics and Heat Transfer*, Vol. 12, No. 4, Oct.–Dec. 1998, pp. 536–542. doi:10.2514/2.6373

[7] Conley, A., Vaidyanthan, A., and Segal, C., "Heat Flux Measurements for GO_2/GH_2 Single-Elemant, Shear Injector," *Journal of Spacecraft and Rockets*, Vol. 44, No. 3, May–June 2007, pp. 633–639. doi:10.2514/1.26678

[8] Beck, J. V., Blackwell, B., and St. Clair, C. R., *Inverse Heat Conduction: Ill-Posed Problems*, Wiley, New York, 1985.

[9] Cook, W. J., and Felderman, E. J., "Reduction of Data From Thin Film Heat Transfer Gauges: A Concise Numerical Technique," *AIAA Journal*, Vol. 4, No. 3, 1966, pp. 561–562. doi:10.2514/3.3486

[10] Cook, W. J., "Unsteady Heat Transfer to a Semi-infinite Solid with Arbitrary Surface Temperature History and Variable Thermal Properties," Iowa State Univ. Engineering Research Inst., TR 67500, Ames, IA, 1970.

[11] Marineau, E. C., and Hornung, H. G., "Modeling and Calibration of Fast-Response Coaxial Heat Flux Gauges," AIAA Paper 2009-737, Jan. 2009.

[12] Oldfield, M. L. G., "Impulse Response Processing of Transient Heat Transfer Gauge Signals," *Journal of Turbomachinery*, Vol. 130, No. 2, April 2008, pp. 1–9. doi:10.1115/1.2752188

[13] Frankel, J. I., Osborne, G. E., and Taira, K., "Stabilization of Ill-Posed Problems Through Thermal Rate Sensors," *Journal of Thermophysics and Heat Transfer*, Vol. 20, No. 2, April–June 2006, pp. 238–246. doi:10.2514/1.9136

[14] Frankel, J. I., "Regularization of Inverse Heat Conduction by Combination of Rate Sensor Analysis and Analytic Continuation," *Journal of Engineering Mathematics*, Vol. 57, No. 2, 2007, pp. 181–198. doi:10.1007/s10665-006-9073-y

[15] Burggraf, O. R., "An Exact Solution of the Inverse Problem in Heat Conduction Theory and Application," *Journal of Heat Transfer*, Vol. 86, Aug. 1964, pp. 373–382.

[16] Groetsch, C. W., "Differentiation of Approximately Specified Functions," *American Mathematical Monthly*, Vol. 98, No. 9, 1991, pp. 847–850. doi:10.2307/2324275

[17] Hanke, M., and Scherzer, O., "Inverse Problems Light: Numerical Differentiation," *American Mathematical Monthly*, Vol. 108, No. 6, 2001, pp. 512–520. doi:10.2307/2695705

[18] Cole, K. D., "Steady-Periodic Green's Functions and Thermal-Measurement Applications in Rectangular Coordinates," *Journal of Heat Transfer*, Vol. 128, No. 7, 2006, pp. 709–716. doi:10.1115/1.2194040

[19] Cole, K., "Green's Functions Library," http://www.engr.unl.edu/~glibrary/home/index.html [retrieved 1 Sept. 2009].

[20] Hensel, E., *Inverse Theory and Applications for Engineers*, Prentice–Hall, Upper Saddle River, NJ, 1991.

[21] Press, W. H., Teukolsky, S. A., Vetterling, W. T., and Flannery, B. P., *Numerical Recipes in Fortran*, 2nd ed., Cambridge Univ. Press, New York, 1993.

[22] Savitzky, A., and Golay, M., "Smoothing and Differentiation of Data by Simplified Least Squares Procedures," *Analytical Chemistry*, Vol. 36, No. 8, 1964, pp. 1627–1639. doi:10.1021/ac60214a047

[23] Oppenheim, A. V., and Schafer, R. W., *Discrete-Time Signal Processing*, Prentice-Hall, Upper Saddle River, NJ, 1989, pp. 39–45.

[24] Moffat, R. J., "Describing the Uncertainty in Experimental Results," *Experimental Thermal and Fluid Science*, Vol. 1, Jan. 1988, pp. 3–17. doi:10.1016/0894-1777(88)90043-X

[25] Skeel, R. D., and M. Berzins, "A Method for the Spatial Discretization of Parabolic Equations in One Space Variable," *SIAM Journal on Scientific and Statistical Computing*, Vol. 11, No. 1, 1990, pp. 1–32. doi:10.1137/0911001

[26] Forsythe, G. E., Malcolm, M. A., and Moler, C. B., *Computer Methods for Mathematical Computations*, Prentice–Hall, Upper Saddle River, NJ, 1976.